Optics Letters

Principle of integrated filtering and digitizing based on periodic signal multiplying

Sitong Wang, Guiling Wu,* Yiwei Sun, and Jianping Chen

State Key Laboratory of Advanced Optical Communication Systems and Networks, Department of Electronic Engineering, Shanghai Jiao Tong University, Shanghai 200240, China
**Corresponding author: wuguiling@sjtu.edu.cn*

Received 28 December 2018; revised 4 March 2019; accepted 4 March 2019; posted 6 March 2019 (Doc. ID 356451); published 28 March 2019

We propose a generic integrated filtering and digitizing approach that can complete signal filtering and digitizing simultaneously based on periodic signal multiplying. The filtering response can be reconfigured flexibly by adjusting the temporal shape of the local periodic signal and/or the impulse response of photodetection. The principle and features of proposed structure are analyzed and experimentally verified in the electrical domain and the photonic domain. The system responses in line with the theoretical and simulation results are experimentally measured.

https://doi.org/10.1364/OL.44.001766

Filtering and digitizing are two basic processes in signal and information fields. For the advantages of digital technology in transmission, processing, and storage, digitizing has become the choice of many applications. Before digitizing, however, pre-filtering is often preferred in many applications for the purpose such as antialiasing, interference suppressing, and phase shifting [1,2]. For example, suppressing interference by pre-filtering can effectively mitigate the requirement of the effective number of bits (ENOB) to analog-to-digital converters (ADCs) in receivers [3]. Conventionally, discrete analog filters and ADCs are cascaded to realize pre-filtering and digitizing, respectively. However, direct cascading an existed microwave photonic filter and a photonic ADC in photonic schemes will suffer from significant loss and distortion for multi-stage electro-optic and optic-electric conversion [4]. In previous works, we have proposed two photonic schemes to digitize RF signals with a programmable equivalent analog pre-filtering by shaping the temporal shape of optical sampling pulses [2,4]. However, the previous works only discussed the photonic structure where the temporal width of the sampling pulse is narrower than the impulse response width of photodetection accounting from the photodiode (PD) to the electric ADC.

In this Letter, we generalize the previous photonic structure to a generic integrated filtering and digitizing principle based on periodic signal multiplying (IFD-PSM). The equivalent model of the IFD-PSM structure is built. The IFD-PSM principle and its features are analyzed under arbitrary temporal shapes of the sampling pulse, and verified in the electrical and photonic domain, respectively.

Figure 1(a) illustrates the generic schematic of IFD-PSM. The input RF signal is multiplied by a local periodic signal. The multiplied signal is filtered by an analog filter and then quantized by an ADC. Finally, the integrated filtering and digitizing results can be directly obtained, and the filtering response can be reconfigured flexibly by adjusting the temporal shape of the local periodic signal and/or the impulse response accounting from the analog filter to the ADC.

The temporal shape of the local periodic signal can be expressed as

$$p(t) = P_A \sum_{m=-\infty}^{+\infty} p_s(t - mT_s), \tag{1}$$

where P_A is the average power of the local periodic signal, $p_s(t)$ is the temporal shape of the periodic signal in single period normalized by P_A, and T_s is the repetition period.

The multiplied signal which is generated by multiplying the local periodic signal and input RF signal, $x(t)$, can be expressed as

$$p_M(t) = p(t)x(t). \tag{2}$$

The multiplied signal is sampled and quantized by the ADC with the sampling period of T_s, and we have the quantized results

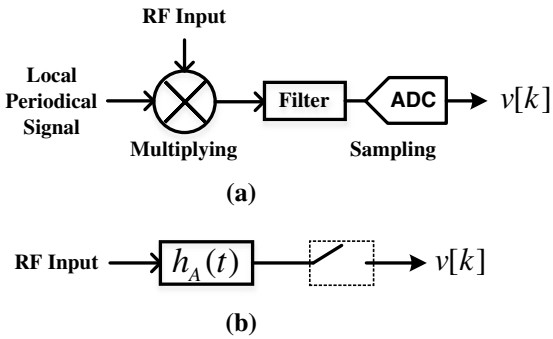

Fig. 1. (a) Generic schematic of the PSM-based integrated filtering and digitizing. (b) Equivalent model of the PSM-based integrated filtering and digitizing.

$$\begin{aligned} v[k] &= p_M(t) * h_E(t)|_{t=kT_s} \\ &= \int_{-\infty}^{+\infty} p(kT_s - \tau)x(kT_s - \tau)h_E(\tau)\mathrm{d}\tau \\ &= \int_{-\infty}^{+\infty} x(kT_s - \tau)p(-\tau)h_E(\tau)\mathrm{d}\tau \\ &= x(t) * h_A(t)|_{t=kT_s}, \end{aligned} \tag{3}$$

where $h_E(t)$ is the impulse response accounting from the analog filter to the ADC. According to Eq. (3), $h_A(t)$ characterizes the equivalent impulse response of the system,

$$h_A(t) = p(-t)h_E(t). \tag{4}$$

Through Eqs. (3) and (4), we can see that the whole procedure can be considered as a sampling system with an equivalent impulse response of $h_A(t)$, as shown in Fig. 1(b). The equivalent response of the system is determined by the local periodic signal's temporal shape and the impulse response of $h_E(t)$.

The equivalent response of the sampling system can be derived from the Fourier transform of Eq. (4) as

$$H_A(\Omega) = \frac{1}{T_s}\sum_{m=-\infty}^{+\infty} P_s(m\Omega_s)H_E(\Omega + m\Omega_s). \tag{5}$$

The functions denoted by an upper case letter are the Fourier transform of the functions expressed by the corresponding lower case letter, $\Omega_s = 2\pi/T_s$. $H_A(\Omega)$ is the weighted summing of the shifted replicas of $H_E(\Omega)$, and the weights are determined by the local periodic signal.

As shown in Fig. 2, the equivalent response of the system can be divided into three categories. It is obvious that since the interval between the shifted replicas of $H_E(\Omega)$ is Ω_s, the adjacent replicas cannot overlap each other and form a continuous passband when the normalized bandwidth of $H_E(\Omega)$ to Ω_s, β_E is less than 0.5. In this case, the system frequency response $H_A(\Omega)$ is composed of multiple discrete passbands whose normalized bandwidths are equal to β_E. Otherwise, β_E is not less than 0.5, and the adjacent replicas can overlap each other and form a continuous passband with a normalized bandwidth much larger than β_E. In this case, the normalized bandwidth of $H_A(\Omega)$ to Ω_s, β, is mainly determined by $P_s(\Omega)$ when the normalized bandwidth of $P_s(\Omega)$ to Ω_s, β_P, is far larger than β_E. With the decrease of β_P, the effect of β_E on β increases, and β will be wider than β_P when β_P is close to or narrower than β_E.

In IFD-PSM, the multiplying process shown in Fig. 1 can be realized by an electrical analog multiplier or an electro-optic modulator. When employing an electrical analog multiplier, the bandwidth of the system will be limited by the bandwidth of the analog multiplier [5]. Benefiting from the merits of

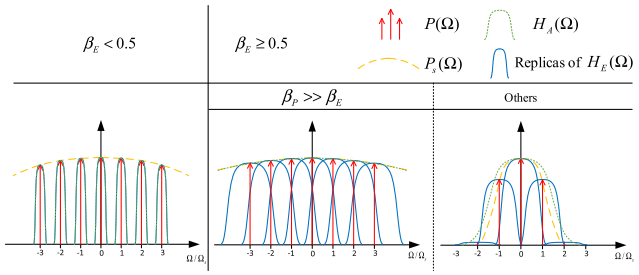

Fig. 2. System frequency responses in three categories.

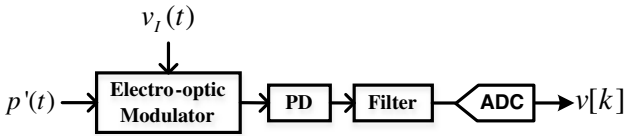

Fig. 3. Photonic scheme. PD, photodiode.

broadband electro-optic modulators, the photonic scheme can improve the system bandwidth significantly. However, the optical signal and optical devices have their own characters that are different from the ideal ones. Therefore, the photonic scheme should be further analyzed.

The photonic scheme using an electro-optic modulator is shown in Fig. 3. Since the temporal shape of the local periodic optical signal, $p'(t)$, can never be negative, it can be expressed as

$$p'(t) = p(t) + b, \tag{6}$$

where b is the amplitude offset to ensure $p'(t)$ is always positive. The lithium niobate Mach–Zehnder modulator (MZM) is usually employed as electro-optic modulator. In the small-signal condition, the response of the MZM biased at quadrature can be approximated linearly [6]:

The modulated signal can be expressed as

$$p_{\mathrm{Mod}}(t) \approx 0.5\alpha[1 - h_{\mathrm{Mod}}(t) * v_I(t)]p'(t), \tag{7}$$

where α is the attenuation factor of the MZM, $h_{\mathrm{Mod}}(t)$ is the small-signal impulse response of the MZM, and $v_I(t)$ is the input RF signal.

In this case, the final sampling result is the sum of an unmodulated part irrelevant to input and the modulated part [7]. The equivalent impulse response of the system can be expressed as

$$h_{A,p}(t) = -0.5\alpha h_{\mathrm{Mod}}(t) * [h'_E(t)p'(-t)], \tag{8}$$

where $h'_E(t)$ is the impulse response accounting from the PD to the ADC. According to Eqs. (6) and (8), the equivalent frequency response of system can be expressed as

$$\begin{aligned} H_{A,p}(\Omega) = {} & \frac{-\alpha}{2T_s}H_{\mathrm{Mod}}(\Omega)\sum_{m=-\infty}^{+\infty} P_s(m\Omega_s)H'_E(\Omega + m\Omega_s) \\ & - \frac{\alpha b}{2}H_{\mathrm{Mod}}(\Omega)H'_E(\Omega). \end{aligned} \tag{9}$$

It is obvious that the bandwidth of the MZM will also limit the bandwidth of system. Compared with the electrical scheme, however, the reachable system bandwidth can be much larger due to the broad bandwidth characteristics of the optical devices. The second item on the right of Eq. (9) illustrates that, due to the offset in $p'(t)$, there is always a passband at the passband location of the analog filter which is usually located at a low frequency. It does not matter when the low frequency interference is weak or a high-pass filter is applied to avoid the low frequency interference.

The experimental setup for the electrical scheme is shown in Fig. 4. The arbitrary waveform generator (AWG) (Keysight, M8195A) produces the local periodic signal which is the product of a periodic Gaussian pulse train and a single tone carrier. Through adjusting the periodic Gaussian pulse train's pulse width, repetition rate, and the single tone carrier's frequency,

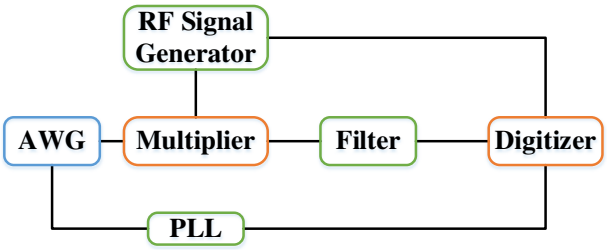

Fig. 4. Experimental setup for the electrical scheme.

the local periodic signal spectrum's bandwidth, frequency interval, and center frequency can be easily designed. The local periodic signal is fed into a multiplier with an analog bandwidth of 500 MHz and multiplied by the sweeping RF signal from a microwave signal generator (Rohde & Schwarz, SMF 100A). The amplitude level of local periodic signal and RF signals are set at 1 V; the spectra of the local periodic signal and RF signals are set under 300 MHz to meet the input requirement of the multiplier. The multiplied signal is then filtered by an analog filter. The filtered signal is finally sampled by a digitizer with an analog bandwidth of 650 MHz and an ENOB of 9.0 (Keysight, M9703A). The frequency of the sweeping RF signal is controlled by the digitizer via LabVIEW. The passband of the analog filter is always located in the passband of the digitizer, so the filtering bandwidth is only limited to the filter bandwidth. The synchronizing signal generated by an AWG is fed into a phase-locked circuit (PLL) to generate the clocks for the digitizer.

Figure 5 shows the measured amplitude frequency responses of a system when $\beta_E < 0.5$. The repetition rate of the local periodic signal is 50 MHz, and a bandpass filter (9.5–11.5 MHz) is used as the analog filter. The full width at half-maximum (FWHM) of the Gaussian pulse and the single tone carrier of the local periodic signals are 12 ns and 150 MHz in Fig. 5(a), respectively. They are 16 ns and 200 MHz in Fig. 5(b), respectively. The calculated spectra of the local periodic signal, $P(\Omega)$, are also presented. We can see that, since $\beta_E < 0.5$, the amplitude frequency responses of system $|H_A(\Omega)|$ in the two cases are both composed of multiple discrete passbands located and weighted by the discrete spectral lines of $P(\Omega)$. Compare Figs. 5(a) and 5(b); the passband's center frequency is shifted from 150 to 200 MHz through adjusting the single tone carrier of the local periodic signal. The weights of the passbands on both sides are also lowered when the FWHM of the Gaussian pulse is changed from 12

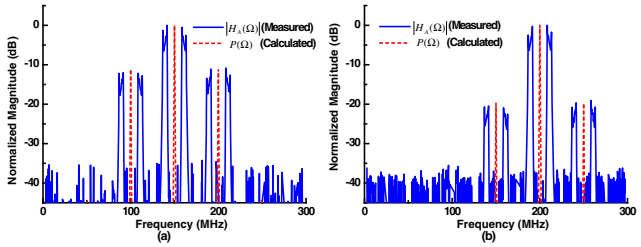

Fig. 5. Amplitude responses in different temporal shapes of the local periodic signal when $\beta_E < 0.5$. (a) Gaussian pulse with the FWHM of 12 ns and a 150 MHz carrier, and (b) Gaussian pulse with the FWHM of 16 ns and a 200 MHz carrier.

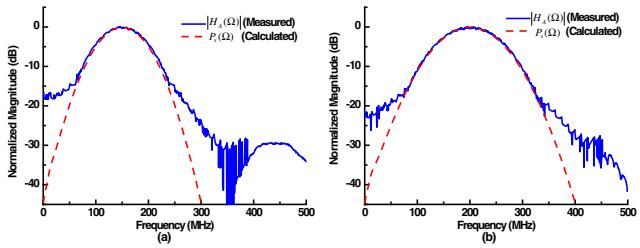

Fig. 6. Amplitude responses in different temporal shapes of the local periodic signal when $\beta_P \gg \beta_E > 0.5$. (a) Gaussian pulse with the FWHM of 8 ns and a 150 MHz carrier, and (b) Gaussian pulse with the FWHM of 6 ns and a 200 MHz carrier.

to 16 ns. This is because the temporal broadening of the Gaussian pulse results in the spectrum compression, and the discrete spectral lines on the both sides of $P(\Omega)$ are lowered.

Figure 6 shows the measured amplitude frequency responses of a system when $\beta_P \gg \beta_E > 0.5$. The repetition rate of the local periodic signal is 12.5 MHz, and a second-order Butterworth low-pass filter (LPF) with an 18.5 MHz bandwidth is used as the analog filter. The FWHM of the Gaussian pulse and the single tone carrier of the local periodic signals are 8 ns and 150 MHz in Fig. 6(a), respectively. They are 6 ns and 200 MHz in Fig. 6(b), respectively. For comparison, the calculated spectra of the local periodic signal in single period, $P_s(\Omega)$, are also presented. Since $\beta_P \gg \beta_E > 0.5$, the amplitude frequency responses of system $|H_A(\Omega)$, in the two cases are formed as a continuous passband and mainly determined by $P_s(\Omega)$. As shown in Figs. 6(a) and 6(b), the measured amplitude frequency responses are consistent with the calculated $P_s(\Omega)$ within the passband. The small deviations between $|H_A(\Omega)|$ and $P_s(\Omega)$ outside the passband may mainly be caused by several non-ideal factors, such as link noises and nonlinearity in the system. The passband's center frequency is shifted from 150 to 200 MHz through adjusting the single tone carrier of the local periodic signal. The passband's bandwidth is also broadened through compressing the FWHM of the Gaussian pulse from 8 to 6 ns.

The experimental setup for the photonic scheme is shown in Fig. 7. The continuous-wave (CW) light generated by a tunable laser is launched into a 20 GHz MZM biased at quadrature with a half-wave voltage of 3.4 V. An AWG (Keysight, M8195A) is employed to generate a periodic electrical signal, which is the product of a 50 MHz periodic Gaussian pulse train with the FWHM of 5 ns and a single tone carrier. The periodic signal is amplified and modulated on the CW light to generate the local periodic optical signal. Another 20 GHz MZM biased

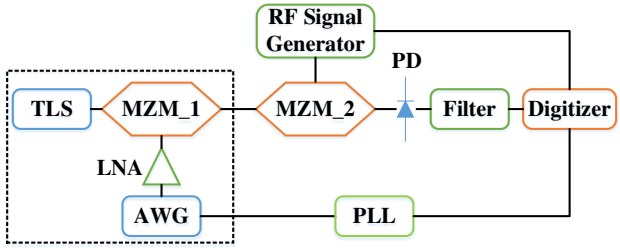

Fig. 7. Experimental setup for the photonic scheme.

at quadrature with a half-wave voltage of 4.5 V is used to modulate the local periodic optical signal by the RF signals generated from a microwave signal generator. The power levels of the AWG output and the RF input are set at −10 m and 0 dBm, respectively, to avoid the nonlinearity of a low noise amplifier (LNA) and MZMs [6]. The modulated signal is detected by a PD with an analog bandwidth of 300 MHz and filtered by a second-order Butterworth LPF with a 74 MHz bandwidth. The filtered signal is finally sampled by a digitizer with an analog bandwidth of 650 MHz and an ENOB of 9.0 (Keysight, M9703A). The frequency of the generated RF signal is controlled by the digitizer via LabVIEW. The synchronizing signal from the AWG is fed into a PLL to generate the clocks for the digitizer.

Figures 8(a) and 8(b) show the measured amplitude frequency responses of a system when the single tone carrier's frequency for the periodic electrical signal is 2.5z and 6 GHz, respectively. For comparison, the simulated passbands based on the temporal shape of the local periodic signal and the impulse response $h'_E(t)$ are also presented. We can see that, since $\beta_P \approx \beta_E > 0.5$, the amplitude frequency responses of system $|H_A(\Omega)|$ are formed as a continuous passband. The passband with the bandwidth of 172 MHz at the center frequency of 2.5 [Fig. 8(a)] or 6 GHz [Fig. 8(b)] can be observed. The bandwidth of the passband is wider than the spectral width of the Gaussian pulse (∼125 MHz). It is because the effect of the photodetection bandwidth increases with the decrease of the local periodic signal's spectral width, and the bandwidth of the passband will be wider than the spectral width of the local periodic signal in this case. One can also see the low passbands equal to that of the LPF (74 MHz) in the two measured results caused by the amplitude offset in the local periodic optical signal $p'(t)$. Compare Figs. 8(a) and 8(b); one can see that the passband's center frequency is shifted from 2.5 to 6 GHz without changing the passband's bandwidth through adjusting the single tone carrier of the local periodic signal. It is because the carrier only determines the location of the local periodic signal's spectrum without changing the local periodic signal's spectral width.

In the experiments above, the output power level of the AWG and microwave signal generator is restricted to avoid the nonlinearity. When the output power level of the AWG is high enough to cause the nonlinearity of the LNA and MZM_1, the harmonics of the designed local periodic signal will appear and be modulated on the CW light. The harmonic components appear in the spectrum of the local periodic optical signal will lead to corresponding passbands in the system response. Figure 9(a) shows the measured amplitude frequency responses of the system when the carrier's frequency of the local

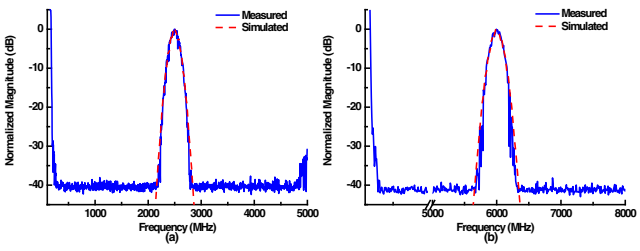

Fig. 8. Amplitude response in different carriers of the local periodic signal when $\beta_P \approx \beta_E > 0.5$. (a) Gaussian pulse with the FWHM of 5 ns and a 2.5 GHz carrier. and (b) Gaussian pulse with the FWHM of 5 ns and a 6 GHz carrier.

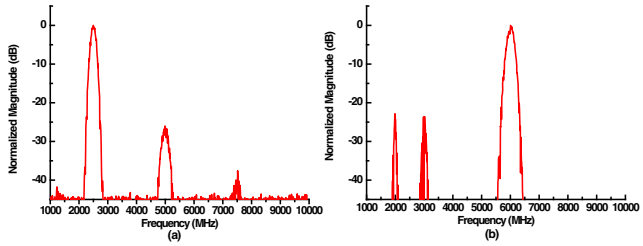

Fig. 9. (a) Amplitude response with the nonlinearity of the LNA and MZM_1 and (b) the amplitude response with the nonlinearity of the small signal amplifier and MZM_2.

periodic signal is set at 2.5 GHz, and the output amplitude of AWG is set at 0 dBm. The passbands located at 5 and 7.5 GHz are corresponding to the designed local periodic signal's second and third harmonics, respectively. The second harmonics is mainly caused by the nonlinearity of an LNA, while the third harmonics is caused by the nonlinearity of an LNA and MZM_1.

Figure 9(b) shows the measured amplitude frequency responses of the system when the carrier's frequency of local periodic signal is set at 6 GHz. and the power levels of input RF signals are set at 20 dBm by adding a small signal amplifier after the microwave signal generator. We can see that, besides the designed passband at 6 GHz, there are two unwanted passbands at 2 and 3 GHz, respectively. The main reason is that the harmonics of the input signal (the third harmonics of 2 GHz and the second harmonics of 3 GHz) caused by the nonlinearity of a small signal amplifier. and MZM_2 in high input powers is located in the designed passband of the system. The second harmonics is mainly caused by the nonlinearity of small signal amplifier, while the third harmonics is caused by the nonlinearity of a small signal amplifier and MZM_2.

In conclusion, we present a generic integrated filtering and digitizing principle based on periodic signal multiplying, which can simultaneously realize signal filtering and digitizing. The equivalent response of the system is determined and can be flexibly configured by the temporal shape of the local periodic signal and/or the impulse response of photodetection. The proposed generic principle is experimentally validated through an electrical scheme and a photonic scheme. The effects of the nonlinearity in the photonic scheme are also discussed.

Funding. National Natural Science Foundation of China (NSFC) (61535006, 61627817).

REFERENCES

1. M. Mishali and Y. C. Eldar, IEEE J. Sel. Top. Signal Process. **4**, 375 (2010).
2. F. Su, G. Wu, and J. Chen, Opt. Lett. **41**, 2779 (2016).
3. J. Capmany, B. Ortega, and D. Pastor, J. Lightwave Technol. **24**, 201 (2006).
4. S. Wang, G. Wu, F. Su, and J. Chen, IEEE Photonics Technol. Lett. **30**, 343 (2018).
5. M. Mishali, Y. C. Eldar, O. Dounaevsky, and E. Shoshan, IET Circuits Dev. Syst. **5**, 8 (2011).
6. J. D. McKinney and K. J. Williams, IEEE Trans. Microwave Theory Tech. **57**, 2093 (2009).
7. F. Su, G. Wu, L. Ye, R. Liu, X. Xue, and J. Chen, Opt. Express **24**, 924 (2016).